Food Hydrocolloids 171 (2026) 111800

Contents lists available at ScienceDirect

Food Hydrocolloids

journal homepage: www.elsevier.com/locate/foodhyd

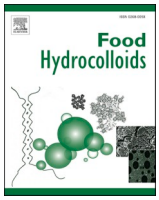

Influence of mono- and divalent cations on heat induced gelation of protein from mealworm (Tenebrio molitor) at various structural length scales

Martina Klost [a,*], Sarah Gleisenberg [a], Stephan Drusch [a], Baohu Wu [b], Olaf Holderer [b], Henrich Frielinghaus [b], Stephan Förster [b], Theresia Heiden-Hecht [b]

[a] Technische Universität Berlin, Faculty III Process Sciences, Institute for Food Technology and Food Chemistry, Department of Food Technology and Food Material Science, Straße des 17. Juni 135, 10623, Berlin, Germany

[b] Jülich Centre for Neutron Science (JCNS) at Heinz Maier-Leibnitz Zentrum (MLZ), Forschungszentrum Jülich GmbH, Lichtenbergstraße 1, 85747, Garching, Germany

ARTICLE INFO

Keywords:
Rheology
SAXS
Insect protein
Scaling
Gelation
Aggregation
Structural changes

ABSTRACT

Mealworm protein gels are promising materials for food or medical applications. Our study aims to elucidate the influence of different salts (NaCl, $MgCl_2$, and $CaCl_2$) on heat-induced gelation of mealworm protein at various structural length scales. Results from rheology, UV–vis and turbidity in fluorescence spectroscopy show an overall increase in aggregation and rheological moduli with addition of ions in the order "no salt" < NaCl < $MgCl_2$ < $CaCl_2$. Prior to heating, this increase is accompanied by an increase of the scattering exponent for $Q <$ 0.01 from SAXS if divalent cations are added, indicating the formation of more compact aggregate structures. Based on results from FT-IR, this can be related to an increase in inter- and intramolecular hydrogen bonding but no specific coordination of the divalent cations with carboxylic groups from the protein side chains can be shown. From scaling of rheological parameters, these additional interactions are derived to occur mainly within the initial flocs rather than between them during the formation of a room spanning gel. Scattering exponents indicate a transition from mass fractals to surface fractals for gels without added salts and gels with NaCl and $MgCl_2$, while the gel structure of gels with added $CaCl_2$ consisted of mass fractals.

1. Introduction

Emerging research on mealworm protein and its thermal gelation contributes to promoting its utilisation in food systems. So far, literature shows the general ability of mealworm protein to form gels at various pH (Klost et al., 2022; Pinel et al., 2024; Zhao et al., 2016) with and without NaCl and with and without added transglutaminase (Zhao et al., 2016). It further shows the gelation behaviour of mealworm protein (and in some cases mealworm protein hydrolysates) in mixture with other proteins like soy (Oh & Kim, 2024; Zhao et al., 2024) and (myofibrillar) pork protein (H. W. Kim, Varankovich, & Nickerson, 2016; T. K. Kim et al., 2020) The dependence of gel strength on heating time and temperature has also been shown (Lee et al., 2019). However, while this research mainly focusses on the influence of those parameters on gelation, there is still a lack of in depth understanding of the underlying structural properties and changes to the protein on the various structural length scales during gelation.

It is generally believed that the thermal gelation of mealworm protein follows the usual path of protein gelation. This includes unfolding upon heating, exposure of previously buried functional groups, intermolecular interactions via these groups and consequently aggregation and – under favourable conditions – gelation. If the resulting gels are particulate in nature, they consist of individual aggregates or flocs, which are connected to each other via interfloc interactions to form an overall room-filling network structure (Mezzenga & Fischer, 2013).

Unfolding, intermolecular interactions, aggregation and gelation may be influenced by various factors such as changes in ionic strength and/or type of incorporated ions. To this regard, the effect of cations is widely acknowledged and is usually more pronounced for divalent cations than for monovalent ones. In this context, Group II cations have previously been described to increase hydrophobicity of hydrophobic areas of the proteins, to interact with a variety of protein surface regions, to form weak interactions with amide bond moieties, to interact with carboxylic protein side chains and to bind to specific cation binding sites of the protein (Asakereh et al., 2022). From a previous study we know,

* Corresponding author.
E-mail address: martina.klost@tu-berlin.de (M. Klost).

https://doi.org/10.1016/j.foodhyd.2025.111800
Received 20 February 2025; Received in revised form 14 July 2025; Accepted 23 July 2025
Available online 24 July 2025

that the addition of $ZnSO_4$ leads to a more particulate structure in mealworm protein gels which resulted in higher rheological moduli and a shorter linear viscoelastic region (Klost et al., 2022).

However, in food applications, the presence of other ions like Na^+, Ca^{2+} and Mg^{2+} is more relevant and occurs more frequently than that of Zn^{2+}. These salts may not only influence the gelation behaviour as part of a formulation. They may also have the potential to be utilised for specific customisation of structural gel properties, as they may be able to stabilise/destabilise proteins and to interact with them to different extents. However, currently, there remains a research gap limiting the understanding of both the mealworm protein gel itself as well as the impact of these ions on gel structure. More specifically this research gap comprises a lack of information on underlying structural rearrangements on a molecular level, e.g. changes in secondary and tertiary structure and changes to defined structures upon addition of cations and heating. The research gap also comprises a lack of information on the fractal dimensions of the resulting aggregates and gels on different length scales and on the contribution of inter- and intrafloc interactions in the gels. This knowledge is, however, necessary to better understand the impact of cations and heating on the structural properties of gels and aggregates of which they are composed. Moreover, there is a lack of additional data on the impact of cations on the rheological properties of the resulting gels.

To contribute to closing this gap, we chose an approach where we added NaCl, $MgCl_2$, and $CaCl_2$ to mealworm protein solutions and examined the structural properties of the protein in these solutions as well as in the corresponding heat-induced gels. To this purpose, protein-cation coordination and heat- and cation-induced changes to the secondary structure of the protein were investigated by FT-IR. Impact of heat and cations on tertiary structure was investigated by intrinsic fluorescence and impact of heat- and cations on absorption at 290 nm by UV–vis spectroscopy. Heat- and cation-induced changes on various length scales were additionally investigated by SAXS and heat- and cation-induced changes to gel structure and changes to rheological behaviour outside the linear viscoelastic regime were investigated by rheology.

2. Material and methods

2.1. Materials

Living mealworms were frozen in liquid nitrogen, lyophilised and stored at ~ −20 °C until extraction. All chemicals were purchased from lab suppliers Carl Roth GmbH (Karlsruhe, Germany) or VWR (Darmstadt, Germany).

2.2. Methods

2.2.1. Extraction of protein from mealworm (T. molitor)

Extraction of proteins was carried out as previously described by Klost et al. (2022). In brief, lyophilised mealworms were ground, subsequently defatted with hexane extracted in distilled water at pH 8 and centrifuged (1850×*g*, 20 min, 20 °C, Avanti J-E with JA-10 fixed angle rotor (Beckman Coulter Brea CA, USA)) followed by lyophilisation of the supernatant (Beta 1–8 LSCplus Christ Gefriertrocknungsanlagen, Osterode am Harz, Germany). The obtained mealworm protein was subjected to a general characterisation and otherwise stored in a refrigerator until further use. The protein content of the lyophilised protein was 67 % (w/w) (protein factor 5.6 (Janssen et al., 2017), determined via DUMAS method), ash content was 9,97 ± 0,19 % (w/w) and residual fat 0,83 ± 0.33 % (w/w) (determined by Soxhlet method). Protein composition was determined by SDS-PAGE and size exclusion chromatography and showed a variety of protein fractions typically associated with muscle (e.g. actin, troponin and myosin), non-muscle and larval cuticle proteins as shown in supplementary material part 3.

2.2.2. Preparation of highly diluted protein solutions for UV–vis and fluorescence spectroscopy

UV–vis and fluorescence spectroscopy was carried out on diluted protein solutions. For UV–vis and fluorescence spectroscopic analysis a protein stock solution of 0.04 % protein was prepared by dissolving 0.3 g of dried mealworm protein (67 % protein content) in 500 ml distilled water. Stock solutions of NaCl, $CaCl_2$ and $MgCl_2$ were prepared at concentrations of 0.6 M. All solutions (protein and salt) were adjusted to pH 7 with 0.1 M NaOH and HCl. Subsequently, 10 mL of the stock solutions were mixed with 10 mL salt solution to obtain solutions with a protein concentration of 0.02 % and 0.3 M salt. Additionally, reference samples were prepared by mixing the protein stock solution with distilled water also adjusted to pH 7. All samples were prepared in triplicate by dilution from the same stock solutions. Before investigation, ~10 mL of each sample was transferred to glass containers. The containers were covered with aluminium foil to avoid evaporation and heated in a drying cabinet at 90 °C for 60 min to induce protein aggregation.

2.2.3. UV–vis spectroscopy

Extinctions of heated and unheated samples with and without Na^+, Ca^{2+} and Mg^{2+} (0.02 % protein and 0.3 M salt where applicable) were measured at wavelengths between 220 and 600 nm in a SPECTROStar Nano photometer (BMG Lebtech, Ortenberg, Germany).

2.2.4. Intrinsic fluorescence

Intrinsic fluorescence of heated and unheated samples with and without Na^+, Ca^{2+} and Mg^{2+} (0.02 % protein and 0.3 M salt where applicable) was measured by excitation of the samples at $\lambda = 290$ nm and scan of emissions between 300 nm $< \lambda <$ 600 nm in a Cary Eclipse Fluorescence Spectrophotometer (Agilent Technologies, Victoria, Australia). For evaluation, the wavelength at maximum emission λ_{max} between 300 and 400 nm as well as the intensity at maximum emission and second order Rayleigh scattering were identified in MS Excel.

2.2.5. Preparation of mealworm protein solutions for all other experiments

Solutions for all rheological experiments as well as for investigations via FT-IR, and SAXS were prepared by dissolving the required amount of protein for final protein concentrations of 9.0 %, 11.2 %, 13.4 %, 15.7 % or 17.9 % (w/w) in 5 mL distilled water (for reference samples), or in 5 mL of 0.6 M NaCl, $CaCl_2$ or $MgCl_2$ solutions for samples with added salt. Subsequently, the pH was adjusted to pH 7 with NaOH and/or HCl (1 M and 6 M) followed by addition of distilled water to a total sample mass of 10 g, thus obtaining samples without salt (reference) or with 0.3 M Na^+, Ca^{2+}or Mg^{2+} concentration and the desired protein concentration. The samples were stirred at room temperature for 1 h with a magnetic stirrer and stored at 4 °C overnight, stirred again and used for further experiments.

All samples for rheological experiments were prepared in triplicate. The exact same solutions (but at 13.4 % (w/w) protein only) were also used for μDSC and FT-IR experiments.

For SAXS experiments one set of each sample was prepared again but at 13.4 % protein content only and 0.01 % sodium azide was added for preservation. For CLSM experiments one set of each sample was prepared at 13.4 % (w/w) protein content only and 20 μL of a 0.2 % solution of rhodamine B was added per gram sample.

2.2.6. Denaturation behaviour by micro difference scanning calorimetry (μDSC)

The same solutions (at 13.4 % (w/w) protein content) that were used for rheological experiments and FT-IR were also investigated in μDSC. To this purpose approximately 500 mg of each solution was filled into an 850 μL Hastelloy® C276 vessel and hermetically sealed. A second vessel was filled with distilled water as a reference. Both vessels were placed into a Micro Calvet Ultra μDSC (Setaram Solutions KEP Technologies SA, Mougins, France) and subsequently held at 20 °C for 600 s, heated from 20 °C to 120 °C at a heating rate of 1.2 K min^{-1}, cooled from 120 °C to

20 °C at a cooling rate of 1.2 K min^{-1} and held for another 600 s at 20 °C. Data was recorded via Calisto Processing software and presented as heat flow over temperature after offset-correction at approximately 34 °C as means of three replicates ± standard deviation.

2.2.7. Molecular structure by fourier transformation infrared spectroscopy (FT-IR)

The same solutions (at 13.4 % (w/w) protein content) that were used for rheological experiments and μDSC were investigated in FT-IR against distilled water as a background. Additionally, gels formed by heating approx. 3 mL of these solution in a 20 mL glass container covered with aluminium foil in a drying cabinet at 90 °C for 30 min were investigated.

FT-IR spectra were recorded at room temperature in the range from 4000 to 800 cm^{-1} on a Bruker Tensor II spectrometer equipped with a liquid nitrogen-cooled mercury-cadmium-telluride detector and a Bio-ATR (attenuated total reflectance) II cell (all Bruker Optic GmbH, Karlsruhe, Germany). Measurements were carried out in triplicate and additionally three times from the same sample. Raw spectra were offset shifted to the intensity at 1455 cm^{-1} (Gerbino et al., 2011) and difference spectra were calculated by (a) subtracting spectra of solutions from those of gels and (b) by subtracting spectra without salts from those with salts. Peak areas for (a) in the amid I and II regions were subsequently calculated in OriginPro 2020b Software (OriginLab Corp., Northhampton, USA). Additionally, peak deconvolution for the identification of νCOO^{-}_{asym} and νCOO^{-}_{sym} vibrations was done in wavenumber ranges of 1595 cm^{-1} to 1550 cm^{-1} and 1390 cm^{-1} (OriginPro 2020b Software (OriginLab Corp., Northhampton, USA)).

More extensive descriptions on the data processing of FT-IR spectra can be found in the supplementary material.

2.2.8. Gelation kinetics

Characterisation of gelation kinetics was done as previously described by Klost et al. (2022). In brief, after storage at 4 °C overnight, the protein suspensions (9.0–17.9 % (w/w) protein, with or without 0.3 M salt) were stirred at room temperature for approximately 1 h and subsequently analysed in temperature sweeps (MCR 502, Anton Paar, Graz, Austria with a concentric cylinder geometry (CC17 bob length 25.013 mm, bob diameter 16.668 mm, cup diameter 18.074), frequency $f = 1$ Hz and intercycle strain $\gamma_0 = 0.1$ %) with heating and cooling rates of 2 K min^{-1} and a holding time of 30 min at 90 °C. Evaporation was avoided by applying a thin layer of silicon oil to the samples' surface and the cup was additionally covered with a lid. Measurements were performed in triplicate.

2.2.9. Characterisation of structural properties of the gels by rheology

Amplitude sweeps for characterisation of the rheological behaviour of the gels (9.0–17.9 % (w/w) protein, with or without 0.3 M salt) were performed at $T = 20$ °C, $f = 1$ Hz and $\gamma_0 = 0.01$ %–1000 %. The limit of the linear viscoelastic regime (LVE) was defined as a 5 % deviation from the initial storage modulus G' at low γ_0 and determined for all samples alongside the initial storage modulus G' within the LVE. For elucidation of the structural properties of the gels we applied the model proposed by Wu and Morbidelli (2001). In brief, we plotted the storage modulus G' within the LVE and the intercycle strain γ_0 at the limit of linearity in a double logarithmic plot over the protein concentration (9.0 %, 11.2 %, 13.4 %, 15.7 % and 17.9 % (w/w)). From the slopes of the respective curves, we calculated the fractal dimension d_f of the gel and the α-value (Wu & Morbidelli, 2001). For evaluation of the rheological behaviour outside the LVE, only results for samples with a protein content of 13.4 % (w/w) were considered. Results are shown as Lissajous curves of intracycle stress τ over intracycle strain γ. Additionally, storage and loss moduli G' and G'' as well as *S- and T-factors* and dissipation ratio φ were plotted over the intercycle strain γ_0. G', G'', *S- and T-factors* were obtained directly from the RheoCompass Software (Anton Paar, Graz, Austria), the dissipation ratio φ was calculated according to Ewoldt et al. (2010).

More extensive descriptions on the rheological investigation, the respective models and equations for result calculations can be found in the supplementary material.

2.2.10. Characterisation of structural properties of the gels by confocal laser scan microscopy (CLSM)

CLSM investigations were performed to visualise the solutions and gels and to validate findings from rheology and SAXS by visual comparison. To this purpose, mealworm protein solutions (13.4 % protein (w/w) and 0.3 M salt where applicable) were dyed with 20 μL of a 0.2 % rhodamine B solution per g sample. Subsequently, 200 μL of the stained solution were pipetted into a chambered coverslip with 8 wells and a #1.5H coverslip like glass bottom (cat. # 80827, ibidi GmbH, Gräfeling, Germany). The slide was covered with aluminium foil and heated in a drying cabinet for 30 min at 90 °C to induce gelation. CLSM was done on a Leica SP8 (Leica Microsystems GmbH, Wetzlar, Germany) with a HC PL APO CS2 63x/1.2 water objective (pinhole at airy unit 1 AU). Emission wavelength for pinhole calculation was 580 nm, the For GFP detection a 3 % (514 nm) laser intensity was coupled with emission detection of 580 nm at a gain of 750 for all solutions and the reference gels as well as the gels prepared with NaCl. For the gels prepared with $CaCl_2$, and $MgCl_2$ a gain of 820 was used. Solutions were measured approx. 10 μm into the sample, gels were measured approx. 15–20 μm into the gel.

2.2.11. SAXS

Small angle X-ray scattering (SAXS) experiments have been carried out at the KWS-X beamline at JCNS, MLZ (Garching, Germany), a XENOCS XEUSS 3.0 XL Garching Version with liquid metal jet source providing Ga-Ka X-rays with a wavelength of $l = 1.314$ Å. All experiments were carried out in a quartz glass capillary (inner diameter 2 mm) on a temperature-controlled stage at room temperature. Heating was done ex-situ with the SAXS measurements performed on the cooled down gels after heating to 90 °C. With SAXS, the Fourier transform of real space correlations are probed in reciprocal Q-space, where the real space length scales d are linked to Q via $Q = 2p/d$. References (Glatter & Kratky, 1982; Gommes et al., 2021) provide information on SAXS and the retrieval of structural information. Fits of the data were made with the sasmodels python module from Sasview 5.0.6. The fits to the data were made with a multi-level Beaucage model (Beaucage, 1996; Hammouda, 2010), and Gaussian peaks for describing a high Q correlation at $Q > 0.5$ $Å^{-1}$. The correlations for the $MgCl_2$ and $CaCl_2$ peaks which emerged at 90 °C at $Q \sim 0.13$ $Å^{-1}$ were also described with a Gaussian fit. The multi-level Beaucage model allows to obtain characteristic length scales from a Guinier radius R_g and fractal dimensions at each length scale region by the slope of the decreasing scattering intensity. It allows to distinguish e.g. between surface and mass fractals via the "Porod exponent" $-p$, with $-p<3$ indicating a mass fractal structure, and $-p>3$ surface fractals. Protein networks for divalent cations indicated in the SAXS measurement are tightly connected to the rheological properties.

2.2.12. Statistic evaluation

Experiments were performed in triplicate, unless stated otherwise in the section above. To determine significant differences between samples with different added ions, results from FT-IR (νCOO^{-}_{asym} and νCOO^{-}_{sym} as well as decreases in peak areas in the amide I and II region), Fluorescence spectroscopy (max. emission intensity of unheated samples) and rheology (G') were evaluated by one way ANOVA preceded by Brown-Forsythe Test to confirm homogeneity of variances and followed by Tukey Post Hoc test. For the UV–Vis absorption a direct inclusion of the effect by heating was possible, consequently, statistic evaluation was done by two-way ANOVA followed by Tukey Post Hoc test. All statistic evaluation was done in OriginPro 2020b Software (OriginLab Corp., Northhampton, USA).

3. Results and discussion

3.1. Protein-cation coordination and other protein stabilising and destabilising effects

The effects cations have on stabilisation and aggregation of proteins may be related to various mechanisms (Asakereh et al., 2022), namely specific coordination between cations and carboxylic side chains, interactions with specific cation binding sites, charge screening with co-occurring decrease of solubility of hydrophobic patches and weak interactions between cations and amide bond moieties.

Specific coordination between cations and carboxylic side chains of glutamic and aspartic acid may be determined by shifts in wavenumbers of the symmetric and asymmetric vibration of carboxyl groups (νCOO^-_{sym} and νCOO^-_{asym}) in the FT-IR spectrum (Fig. 1). For our samples the addition of salts did not lead to significant shifts in wavenumbers in the νCOO^-_{asym} region and in the νCOO^-_{sym} region (Table S1). Observed shifts were distinctly smaller than values given in literature for specific types of ion coordination (Deacon & Phillips, 1980). Therefore, we do not assume any specific kind of protein-ion coordination involving carboxylic side chains in our study. Instead, it is likely that added cations in our samples are responsible for changes in protein stabilisation and aggregation by other mechanisms. These mechanisms were summarised by Asakereh et al. (2022) and will be briefly discussed based on literature reports in the following paragraphs.

Specific cation binding sites have been shown for various muscle proteins. G-actin has been reported to contain a high affinity Ca^{2+} binding site and three moderate affinity sites and to also be able to bind Mg^{2+}, which in turn promotes filament assembly of actin (Zimmerle et al., 1987). Troponin has been reported to contain two sites that can bind Ca^{2+} or Mg^{2+} competitively and two Ca^{2+} specific sites as well as two Mg^{2+} specific sites (Potter & Gergely, 1975). Regarding our study, the fact that we are looking at a system of mixed proteins makes it difficult to allocate the impact of Ca^{2+} or Mg^{2+} binding to specific binding sites or protein fractions. However, it needs to be assumed, that this does take place, since the utilised salt concentrations in our study (0.3 M) are distinctly higher, than those required for binding to these sites (200 μM–1 mM (Zimmerle et al., 1987)).

Charge screening and decrease of solubility of hydrophobic patches should have a stabilising effect (Asakereh et al., 2022) and may be assumed to play an unspecific role in our study. Cations may screen negative charges without any specific coordination. At the same time chloride anions would screen any positive charges, that remained above the isoelectric point (pI). In this context different chloride concentrations in NaCl (0.3 M) and $MgCl_2$/$CaCl_2$ (0.6 M) must be considered. Additionally, hydrated Ca^{2+} or Mg^{2+} ions may immobilise water and therefore contribute to local salting out effects in the vicinity of hydrophobic moieties (Asakereh et al., 2022).

Protein destabilising effects owing to weak interactions between cations and amide bond moieties cannot entirely be ruled out in our study and – if present – would promote the unfolded state. However, salt concentrations under which this effect could be clearly observed appear to be distinctly higher (lowest tested concentration by Asakereh et al. (2022) was 2 M) than in our study.

3.2. Heat- and cation induced changes to secondary structure by FT-IR

From the FT-IR raw spectra of our samples in Fig. 1 it becomes apparent that the amide I (wavenumbers between 1600 and 1700 cm^{-1}) and amide II (wavenumbers between 1480 and 1600 cm^{-1}) bands are

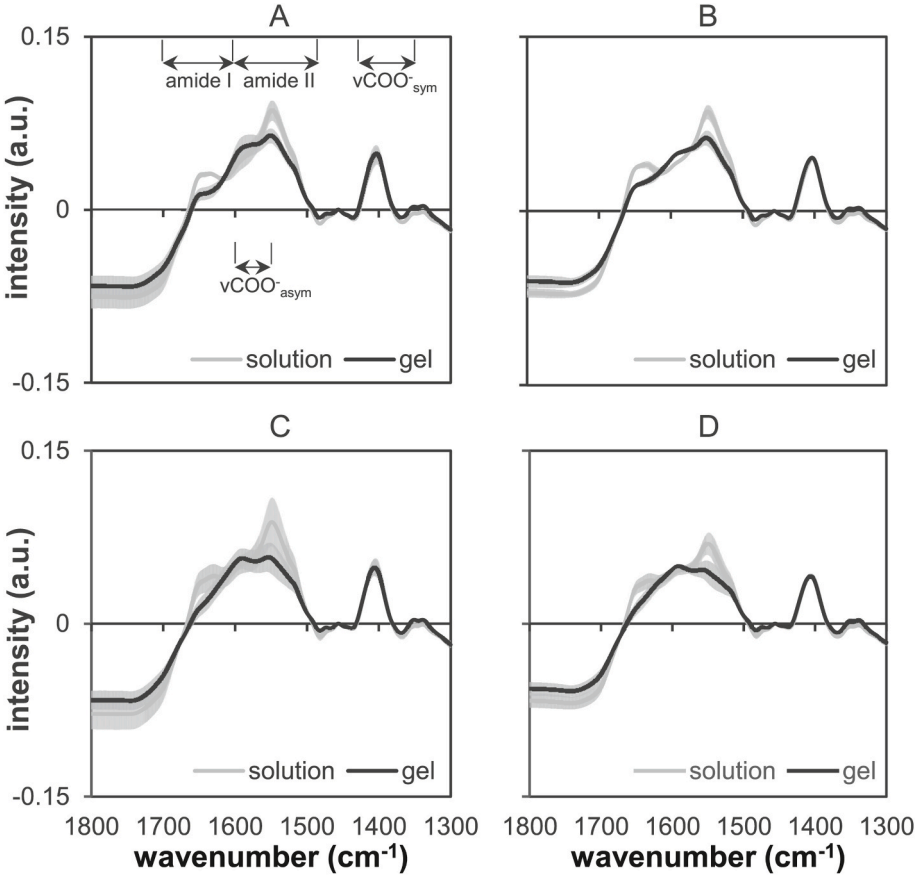

Fig. 1. Raw spectra from FT-IR analysis of mealworm protein solutions and gels with a protein content of 13.4 % (w/w) with and without the addition of various ions. (A = reference, B=NaCl, C=$MgCl_2$, D = $CaCl_2$). Error bars represent the standard deviation of three individual samples.

not very well resolved. This may be caused by non-protein constituents of the sample, especially at wavenumbers around 1600 cm^{-1}. To diminish this effect, and to better resolve changes, difference spectra were calculated.

To resolve heat induced structural changes during gelation, difference spectra were obtained by subtracting the raw spectra of protein solutions without or with addition of salts from those of the corresponding gels (Fig. 2). All difference spectra show negative peaks in the amide I and II regions, indicative of structural changes related to heat-induced unfolding of the protein. Comparison of peak areas of the difference spectra between samples did not show a significant influence of salt addition on the extent of heat induced structural change (Table S2). While these difference spectra only display structural changes during sol-gel transition for each sample, they do not reflect salt-induced differences between samples either in solution or in the gel state.

To resolve the salt-induced changes, additional difference spectra obtained by subtracting the spectra of the reference sample from the spectra of the respective samples with the added salts were considered for both, solutions and gels (Fig. 3). Results revealed an increase in secondary structure elements in solutions and gels upon the addition of salt. Positive values in Fig. 3 indicate an increase in hydrogen bonds through an increase of the respective secondary structure elements at the corresponding wavenumbers (>1670 cm^{-1} = intramolecular β-sheets, 1648 to 1658 cm^{-1} = α-helices, 1630 to1640 cm^{-1} = intramolecular β-sheets, 1610-1628 cm^{-1} = intermolecular β-sheets, according to Jackson and Mantsch (1995)). More specifically, the nature of this increase differs depending on the type of salt. In this regard, the addition of NaCl to led to an increase of all secondary structure elements in both, unheated solutions and gels. This increase was most pronounced at wavenumbers indicative of intramolecular β-sheets (Fig. 3 A) and not affected by thermally induced gelation.

The addition of $MgCl_2$ (Fig. 3 B) led to a less pronounced increase at wavenumbers indicative of α-helices and a more pronounced increase at wavenumbers indicative of β-sheets. Upon gelation distinct (but overall not significant) changes occurred especially at wavenumbers representing α-helices. Additionally, a slight shift of peaks related to β-sheets to higher wavenumbers indicates an overall weakening of the hydrogen bonds (Jackson & Mantsch, 1995).

Upon addition of $CaCl_2$ (Fig. 3 C) the tendency observed for samples with NaCl and $MgCl_2$ continues. More specifically, the increase at wavenumbers indicative of α-helices is less pronounced and the increase at wavenumbers indicative of β-sheets is more pronounced with added $CaCl_2$. Heat induced gelation led to distinctly (but overall not significantly) larger values of difference spectra at wavenumbers related to β-sheets and a shift of those peaks to higher wavenumbers which (as described for samples with $MgCl_2$) indicates an overall weakening of hydrogen bonds in these samples, too (Jackson & Mantsch, 1995).

In summary, the addition of salts led to an increase of secondary structure elements and therefore to an increase of hydrogen bonds while thermal gelation led to an overall decrease in structural elements.

3.3. Heat- and cation induced changes to tertiary structure by intrinsic fluorescence and UV–vis spectroscopy at 290 nm

To assess tertiary structure changes induced by salt addition and/or heat treatment, intrinsic fluorescence measurements were conducted on highly diluted protein samples. These conditions effectively reveal structural alterations in solution and during early aggregate formation. Closed lines in Fig. 4 show the emission spectra of heated and unheated mealworm protein solutions. The emission spectra are complemented by absorption spectra from UV–vis spectroscopy (open lines) and photographs of the examined samples. As can be seen on a glimpse, samples with added $MgCl_2$ or $CaCl_2$ became turbid owing to pronounced protein aggregation upon heating. This led to increased absorption at 290 nm and increased second order Rayleigh scattering (peak at ~580 nm). In combination, this implies inner filter effects which in turn cause a decrease in emission intensity that cannot be distinguished from decreases in emission intensity caused by quenching. Consequently, we

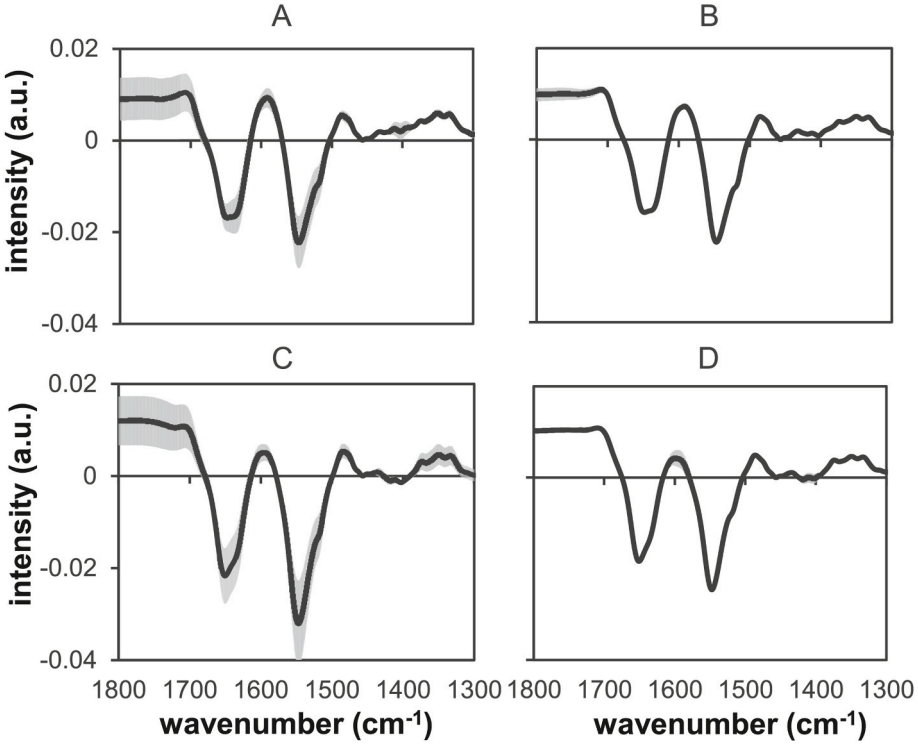

Fig. 2. *Difference spectra from FT-IR analysis of mealworm protein with and without the addition of 0.3 M ions at a protein concentration of 13.4 %, obtained by subtracting the raw spectrum of the solutions from the raw spectrum of the gels (A = reference, B=NaCl, C=$MgCl_2$, D = $CaCl_2$). Errorbars represent the standard deviation of three individual samples.*

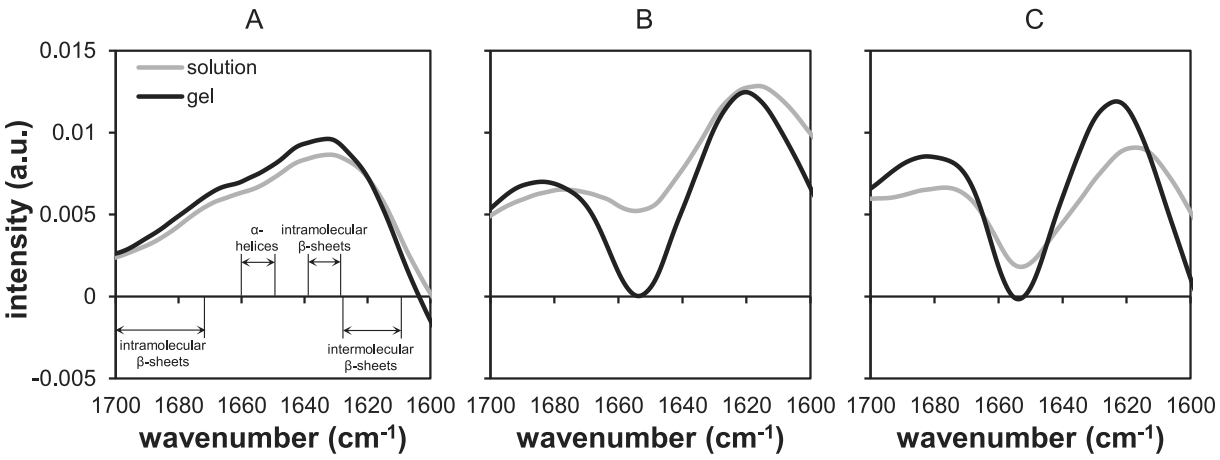

Fig. 3. FT-IR difference spectra for solutions and gels with and without the addition of 0.3 M ions at a protein concentration of 13.4 % in the amide I region (wavenumber range from 1700 cm^{-1} to 1600 cm^{-1}) obtained by subtracting the raw spectrum of the reference sample from the raw spectra of the respective samples with NaCl (A), $MgCl_2$ (B) or $CaCl_2$ (C). Assignment of wavenumbers to structural elements according to Jackson and Mantsch (1995).

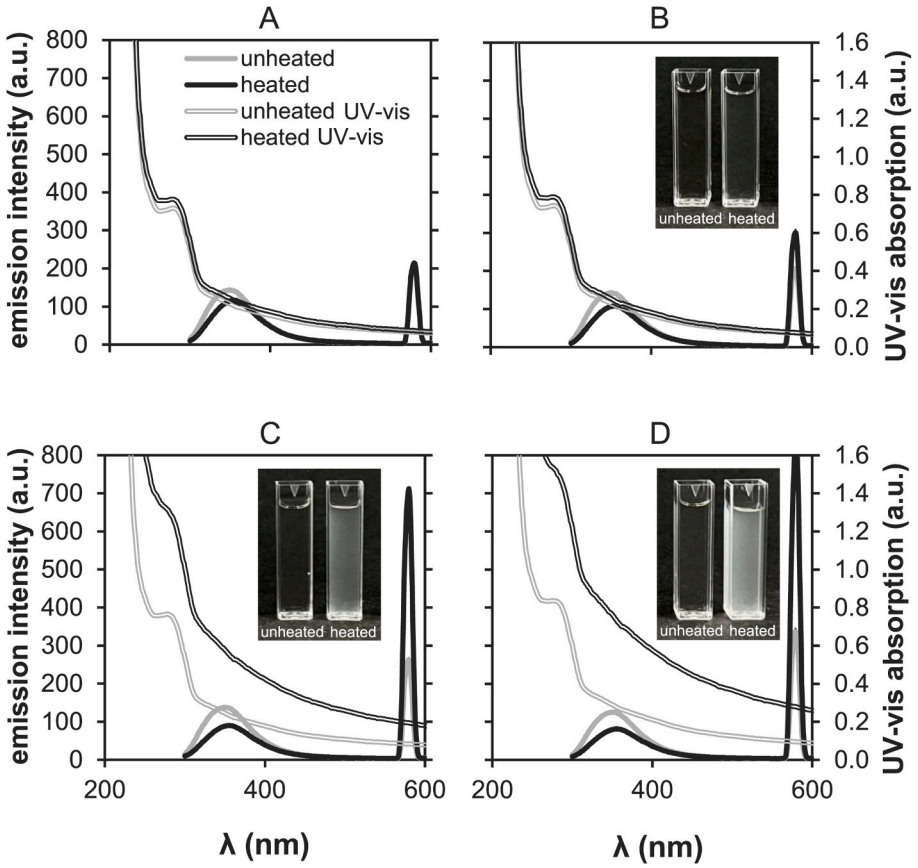

Fig. 4. UV–vis spectra (open lines) and emission spectra from fluorescence spectroscopy (closed lines) of highly diluted, heated and unheated samples (0.02 % protein and 0.3 M salt concentration). Excitation for intrinsic fluorescence measurements was carried out at 290 nm. Inset: photograph of the corresponding samples. (A = reference, B=NaCl, C=$MgCl_2$, D = $CaCl_2$).

will not discuss changes to the emission intensity (Table S3) in our study with regard to changes in tertiary structure of the protein.

We will, however, discuss the maximum emission wavelength $\lambda_{max.\ intensity}$ and changes thereof (Table S3). $\lambda_{max.\ intensity}$ of unheated samples was approx. 350 nm with no significant differences between samples. Emission wavelengths for proteins are usually in the range between 330 nm for mostly folded proteins and 360 nm for mainly unfolded proteins (Vladislav Victorovich et al., 2021). Consequently, from the $\lambda_{max.\ intensity}$ at 350 nm, we conclude an already mainly unordered tertiary structure with distinct exposure of the tryptophan residues in unheated solutions and independent of added salt. On the one hand, this may be related to the not very compact structure of many muscle proteins (e.g. UniProt entries Q8T6L6 and A0A0B4KGR6). On the other hand, some pre-damage of the protein during mealworm storage, protein extraction and processing may have taken place and contributed to further protein unfolding.

Upon heating and subsequent cooling, the $\lambda_{max.\ intensity}$ underwent a significant red shift to values between ~354.1 ± 1.0 and 356.6 ± 1.7 nm

for all samples (Fig. 4 and Table S3). This is indicative of an increased exposure of previously buried tryptophane residues to the more polar environment of the solvent (i.e. water or salt solutions) and therefore further loosening of the tertiary structure in all samples (Duy & Fitter, 2006). Since the red shift is similar for all samples, it can be assumed that the addition of salt does not significantly influence the unfolding of the protein on the tertiary structure level upon heating.

Consequently, in combination with results from FT-IR, we propose a molecular structure that involves some secondary structure elements (more so in the presence of salts), but is rather unordered on the tertiary structure level, thus exposing the tryptophan residues in protein side chains. The more pronounced turbidity and aggregation in samples with $MgCl_2$ or $CaCl_2$ is most likely related to charge screening effects and/or immobilisation of water and resulting local salting out effects.

3.4. Heat and cation induced changes on various length scales by SAXS

SAXS measurements can be utilised to obtain structural information on various length scales of the protein gel. Our results (Fig. 5) imply multiscale structures, as indicated by the lack of a plateau in the lower Q (<0.003 Å^{-1}) region. Additionally, a lack of form factors in the region at Q ~ <0.01 Å^{-1} allows for the calculation of the „Porod Exponent" that corresponds to the fractal dimensions of aggregate structures at the respective length scale and a deviation from a pure power law at Q > 0.1 Å^{-1} allows for the description of characteristic sizes represented by corresponding radii of gyration R_g.

At Q > 0.1 Å^{-1}, we found two spherical form factors (from the Beaucage model) with radii of gyration R_{g1} of ~3.4–7.1 nm and R_{g2} ~1.3–2.1 nm (Fig. 5, Table S4). These form factors were present in all solutions independent of added salt. R_{g2} might be related to actin monomers that were previously reported with radii of 19.9 (Goddette et al., 1986) to 27 ± 1 Å (Norman et al., 2005) or to aggregates of protein fractions with distinctly smaller molecular weights. A clear distinction between the two is not possible, owing to the complex protein mixture in the samples. R_{g1} may consist of actin dimers that have been proposed at 29 (Goddette et al., 1986) to 52 Å (Norman et al., 2005) or other monomeric proteins or small aggregates. All other protein fractions appear not to be present in regular structures and may instead be part of multi-scale structures. In unheated solutions, R_{g2} was lower for samples with $CaCl_2$ possibly indicating a denser structure.

Regarding the impact of heating during thermal gelation, results did not show any structural changes for the reference and the sample with added NaCl. In contrast, heat induced gelation of samples with added $MgCl_2$ resulted in the decrease of R_{g2} and the formation of an additional, well pronounced correlation peak at $Q = 0.13$ Å^{-1}, indicating a regular structure with a repeat distance of $d = 2p/Q = 4.8$ nm and a radius of gyration R_{g1} of 71 ± 10 Å. With $CaCl_2$, only a very broad peak at about the same Q indicating weak ordering with large heterogeneity arose after heating to 90 °C during gelation. It has been observed that actin filaments can result in such peaks at Q = 0.1–0.13 Å^{-1} (Töpperwien et al., 2016), which also depend on counterion organisation (Angelini et al., 2005).

The observed overall changes to small, defined structures as determined by SAXS and to tertiary and secondary structures (derived from fluorescence spectroscopy and FT-IR respectively) upon heating would also be expected to be reflected in the denaturation temperature and enthalpy (Fig. 6). For the reference sample and the samples with added NaCl and $CaCl_2$ the distinctly high $\lambda_{max.\ intensity}$ in the unheated state and

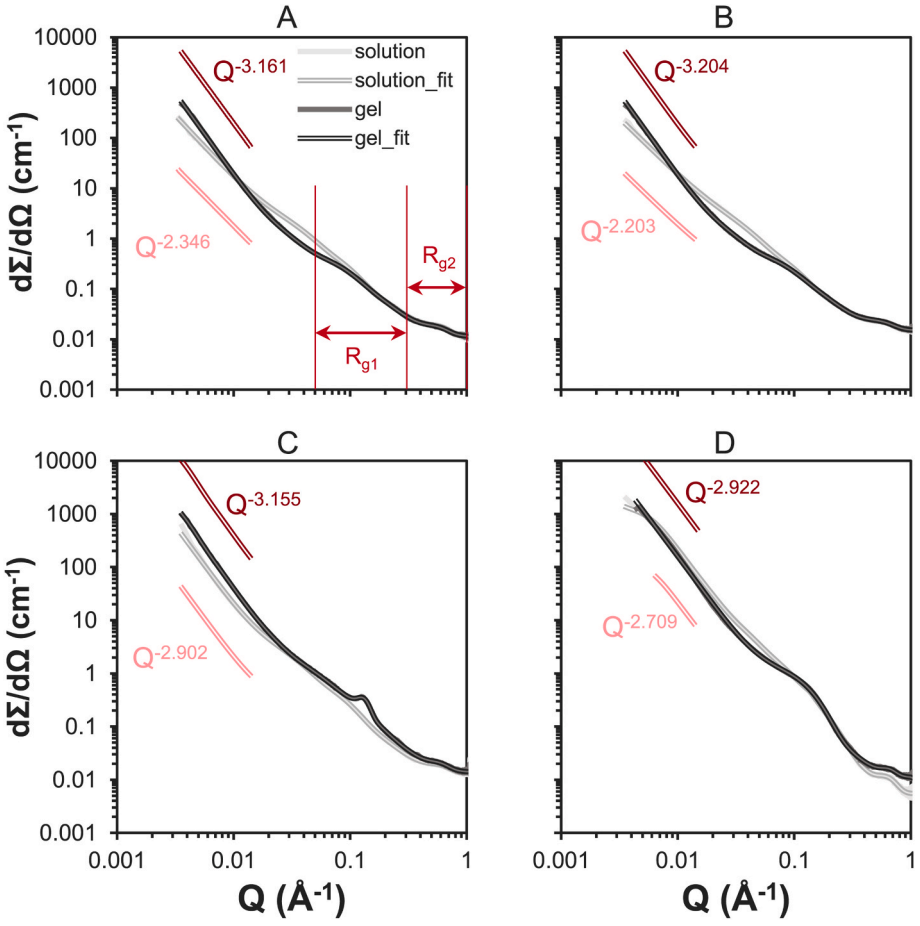

Fig. 5. SAXS results for the protein solution and for the gels after heating with and without the addition of 0.3 M ions at a protein concentration of 13.4 %. (A = reference, B=NaCl, C=$MgCl_2$, D = $CaCl_2$).

the relatively small red shift upon heating (both observed in fluorescence spectroscopy, Fig. 4) is in agreement with results from μDSC measurements (Fig. 6) where no specific denaturation peak could be found and overall denaturation enthalpy was not very pronounced. The more pronounced denaturation curves for samples with $MgCl_2$ may be related to the development of ordered structures of $R_{g1} = 71 \pm 10$ Å that may to some extent be caused by binding of Mg^{2+} to various calcium specific binding sites in the actin (Frieden, 1983; Zimmerle et al., 1987). This binding of Mg^{2+} to calcium specific binding sites was previously described to cause the formation of actin trimers and subsequent filaments (Frieden, 1983). However, it remains unclear how this relates to the $\lambda_{max.\ intensity}$ in fluorescence spectroscopy which was similar to all other samples and findings from changes to secondary structure from FT-IR that did also vary only slightly from the other samples. One possible explanation would be a similar impact of Mg^{2+} and Ca^{2+} on the secondary structure upon binding to the Ca^{2+} specific binding sites as would be supported by results in Fig. 3 (difference spectra from FT-IR in the amid I region) and aggregation without relevant displacement of tryptophan residues from aqueous environment.

On an intermediate scaling level (Q~<0.01 $Å^{-1}$), flocs (also known as aggregates) form via various interactions and constitute the building blocks of the gel. To obtain further information on these structures, the scattering exponents p at Q~ <0.01 $Å^{-1}$ (corresponding to structures between ~60 and 600 nm in size) were considered for solutions and gels. These scattering exponents p correspond to the fractal dimensions of flocs in the corresponding length scale according to Hammouda (2010).

$$intensity = \frac{d\Sigma}{d\Omega} \propto Q^{p}$$

On the length scale of the flocs, the sample is a mass fractal with fractal dimension $D_m = -p$ if $-p < d$ and a surface fractal with fractal dimension $D_S = 6+p$ if $d < -p < d+1$, d is the Euclidean dimension (Beaucage, 1996; Hammouda, 2010).

Regarding our samples, in the unheated state the scaling exponents were −2.346 (reference), −2.203 (NaCl), −2.902 ($MgCl_2$) and −2.709 ($CaCl_2$) (Fig. 5). This indicates that all solutions contain flocs that may be considered mass fractals on the corresponding length scale. The closer the fractal dimension D_m of a mass fractal is to the Euclidean dimension d, the denser is the corresponding floc structure. Consequently, we can assume the protein to assemble in fairly lose and open flocs if NaCl or no salt is added to the sample (as indicated by fractal dimensions D_m of 2.2–2.35), while the presence of $MgCl_2$ or $CaCl_2$ leads to the formation of denser flocs with fractal dimensions D_m close to d ($D_m = 2.902$ ($MgCl_2$) and $D_m = 2.709$ ($CaCl_2$). Denser flocs upon the addition of $MgCl_2$ or $CaCl_2$ may be caused by (unspecific) charge screening and increased hydrophobicity of hydrophobic moieties (Asakereh et al., 2022). These may lead to fewer repulsive forces in the flocs and consequently closer packing within the flocs. Furthermore, additional hydrogen bonds may occur in samples with divalent cations as indicated by the increase in intermolecular β-sheets as shown in Fig. 3.

In the gelled samples scattering exponents - were −3.161 (reference), −3.204 (NaCl), −3.155 ($MgCl_2$) and −2.922 ($CaCl_2$) (Fig. 5). For the reference sample and the samples with added NaCl or $MgCl_2$ $d < -p < d+1$. Consequently, on the length scale of the flocs, we are looking at surface fractals. In general, surface fractals indicate the smoothness of interfaces between the sample mass and the pores. The closer the scattering exponent is to d (we are looking at a three-dimensional system, therefore d = 3) the rougher is the interface in question. The closer $-p$ is to d+1, the smoother the interface (Anitas, 2020). Consequently, reference gels and gels with added NaCl or $MgCl_2$ display a distinctly rough, albeit quite defined interface between the protein-network and the enclosed pores. In contrast, the scattering exponent for the sample with added $CaCl_2$ is just below three ($p = -2.922$) and therefore a mass fractal, with a fractal dimension D_m that indicates a compact structure close to the transition to surface fractal. This specific behaviour of the $CaCl_2$ containing sample is to some extent in agreement with the pronounced aggregation behaviour indicated by increased turbidity described above (Fig. 4) and might indicate a gel structure, that is dominated by these aggregates.

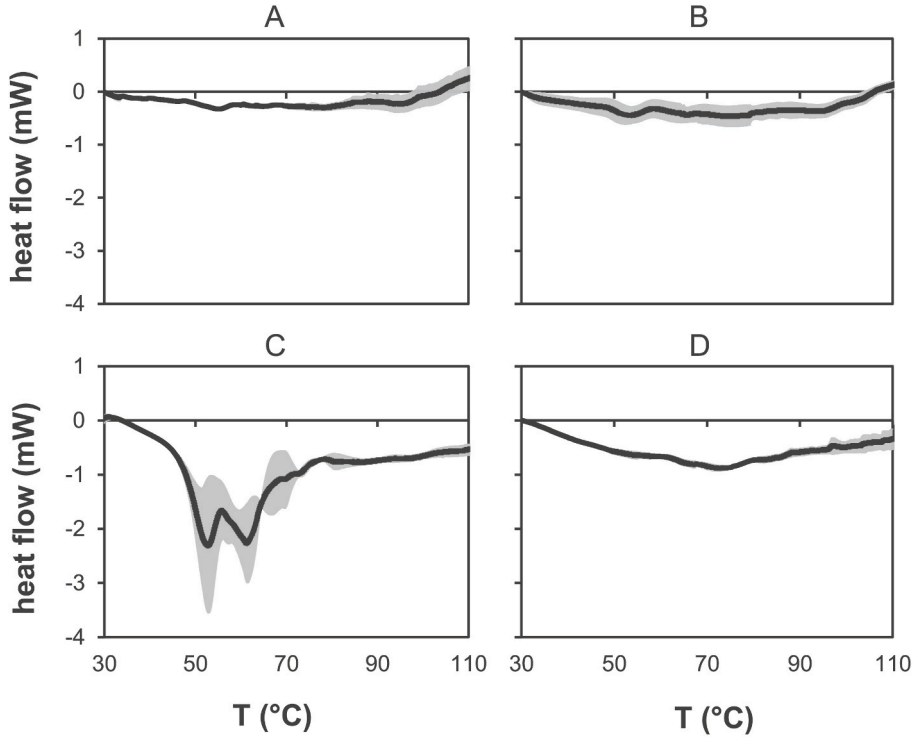

Fig. 6. μDSC thermograms of 13.4 % (w/w) protein solutions with and without the addition of 0.3 M NaCl, $MgCl_2$ or $CaCl_2$. Heating rate was 1,2 K min^{-1} (A = reference, B=NaCl, C=$MgCl_2$, D = $CaCl_2$).

3.5. Heat and cation induced changes to gel structure by rheology

Temperature sweeps (depicted as storage and loss moduli G' and G'' in Fig. 7) allow to follow the formation of the gel structure. At a protein content of 13.4 %, all samples showed an increase in G' (and G'') during heating and cooling. During heating, the protein unfolds partially, intramolecular disulfide bonds may get disrupted and previously buried – often hydrophobic – areas of the molecule become exposed. To decrease the entropy of the surrounding water molecules, new hydrophobic interactions form between different molecules (J. H. J. Kim, Varankovich, & Nickerson, 2016). In addition, exposed sulfhydryl-groups may form intermolecular disulfide bonds (J. H. J. Kim, Varankovich, & Nickerson, 2016). During holding this process may continue and ultimately reach a stable state. During cooling, the formation of short-range interactions such as hydrogen bonds and van der Waals interactions are favoured (Chronakis, 2001) and further increase G'. From gel solubility experiments in a previous study, we determined that the interactions stabilising heat-induced mealworm protein gels were mainly non-covalent and consist mostly of hydrophobic interactions and hydrogen bonds (Klost et al., 2022).

At the end of the temperature sweep, G' was significantly higher for samples with added Ca^{2+} and Mg^{2+} compared to the sample with added Na^{+} and the reference. These results are in agreement with reports on the impact of $MgCl_2$ and $CaCl_2$ on gel hardness of soy protein gels, where a higher coagulation power was described for Ca^{2+} in comparison to Mg^{2+} (Li Tay et al., 2006). They are also in agreement with our previous study, where the addition of $ZnSO_4$ (0.3 M) led to higher G' values and an overall decrease in gel solubility indicating the formation of additional interactions, that may be ionic or covalent (Klost et al., 2022) and involve protein fractions < approx. 20 kDa that were previously not part of the gel (unpublished data). Consequently, we assume the most/largest aggregates in gels with added $CaCl_2$ followed by those with $MgCl_2$. This is also supported by the fractal dimensions of the gels at the floc length scale from SAXS, that indicate a more aggregate-dominated overall structure especially with added $CaCl_2$. Gels prepared with protein concentrations of 9.0 %, 11.2 %, 15.7 % and 17.9 % protein showed similar gelation kinetics.

Values for G' at the end of gelation for all concentrations are shown in Fig. 8 (and Table S5), where they are plotted over the protein concentration as part of the scaling model by Wu and Morbidelli (2001). This scaling model allows us to investigate the contribution of intra- and interfloc interactions in the gels as well as to examine the overall fractal dimensions d_f of the gels (Fig. 8, Table 1). Results showed similar fractal dimensions d_f for the reference and the NaCl containing sample (~2.3) as well as similar fractal dimensions d_f for the samples with added divalent cations (~2.45). Overall, these numbers are in agreement with values shown by Wu and Morbidelli (Wu & Morbidelli, 2001) for various protein gels. The differences in fractal dimensions d_f between the samples confirm the denser network structure implied by higher G' values at the end of the temperature sweeps and the development of a regular structure upon heat induced gelation for samples with added $MgCl_2$ or $CaCl_2$ as shown in SAXS experiments.

To additionally investigate the contribution of interactions within the flocs in relation to those between the flocs, we calculated the α-values according to Wu and Morbidelli (2001). α is a constant in the range of $0 < \alpha < 1$ and indicates the contribution of intrafloc and interfloc interactions, with $\alpha = 0$ indicating a system ruled by interfloc interactions and $\alpha = 1$ indicating a system ruled by intrafloc interactions. Values in between indicate network structures where both types of interactions contribute (Wu & Morbidelli, 2001). To this regard, the addition of salts led to a shift towards a larger contribution of intrafloc interactions (increase in α) (Table 1). This was more

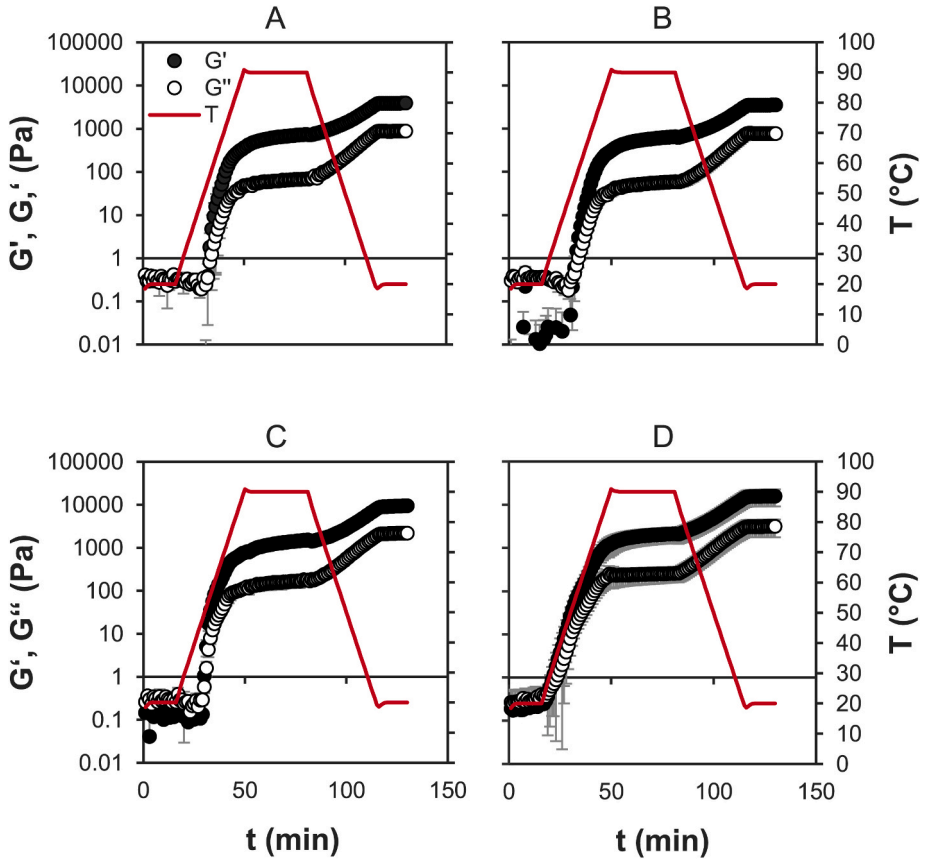

Fig. 7. Storage and loss moduli G′ and G'' from temperature sweeps of mealworm protein solutions with and without the addition of 0.3 M ions at a protein concentration of 13.4 %. f = 1Hz, γ_0 = 0.1 %. Results are means of triplicate determination, errorbar represent the standard deviations. (A = reference, B=NaCl, C=$MgCl_2$, D = $CaCl_2$).

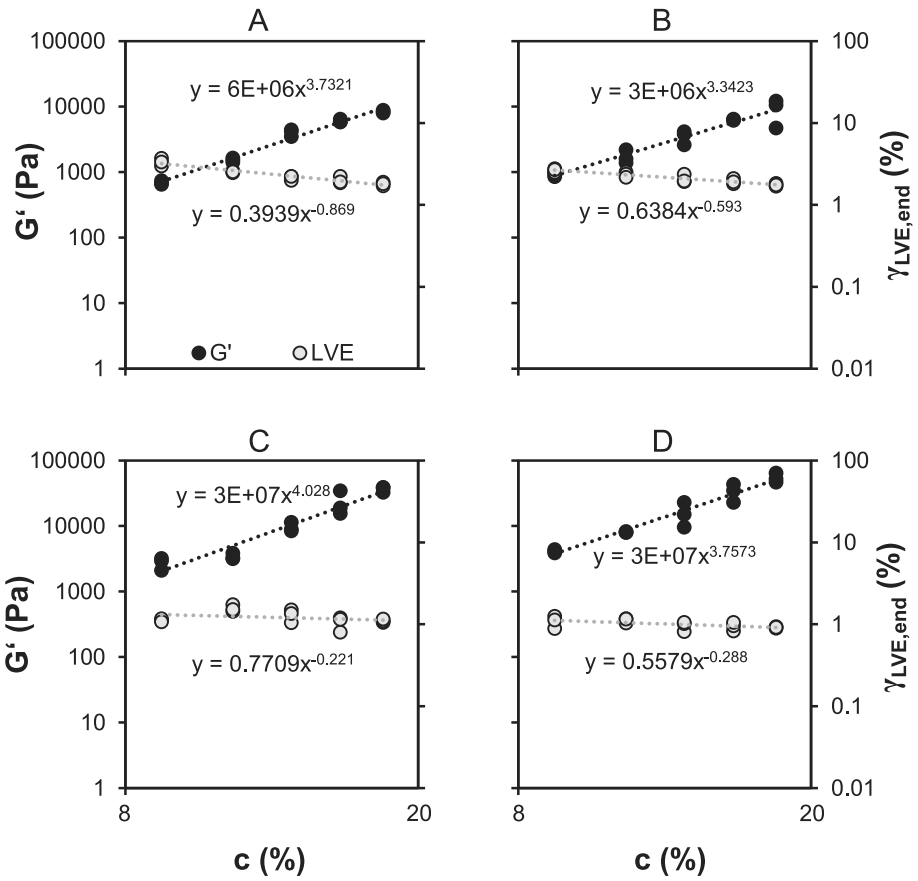

Fig. 8. Storage modulus G′ of mealworm protein gels with and without the addition of 0.3 M ions in the linear viscoelastic regime and intercycle deformation at the end of the linear viscoelastic regime, both obtained from amplitude sweeps, plotted over the protein concentration. (A = reference, B=NaCl, C=$MgCl_2$, D = $CaCl_2$).

Table 1
Fractal dimensions d_f and α-value calculated from the slopes of storage modulus G' and the intercycle deformation at the end of the linear viscoelastic regime according to the model by Wu and Morbidelli (Wu & Morbidelli, 2001).

sample	d_f	α
reference	2.30	0.51
Na^+	2.27	0.57
Mg^{2+}	2.47	0.66
Ca^{2+}	2.42	0.65

pronounced if divalent cations were used, but independent of type of divalent cations, even though results from SAXS indicate a more aggregate dominated structure with Ca^{2+} than Mg^{2+} based on the fractal dimensions D_m and D_s respectively at the floc length scale. When considering the α-values in combination with the G' and d_f, which are an indication of network density (and may therefore be related to the number of interactions), the scattering exponents -p from SAXS for information on interfacial structure and all previous considerations on the other structural levels we propose the following mechanisms:

On tertiary structure level, proteins are already fairly unfolded, consequently already exposing functional patches that may interact with each other, when charges are screened as is the case if (divalent) cations are added. On secondary structure level, intermolecular β-sheets increase if (divalent) cations are added, indicating an increase in hydrogen bonding between molecules. Therefore, addition of divalent cations leads to overall denser aggregates. This is most likely caused by less repulsion, corresponding promotion of protein-protein interactions and incorporation of additional protein fractions. Additional protein-protein interactions and incorporation of protein occur mainly within the flocs and only to a lesser extent between the flocs. Owing to the increased

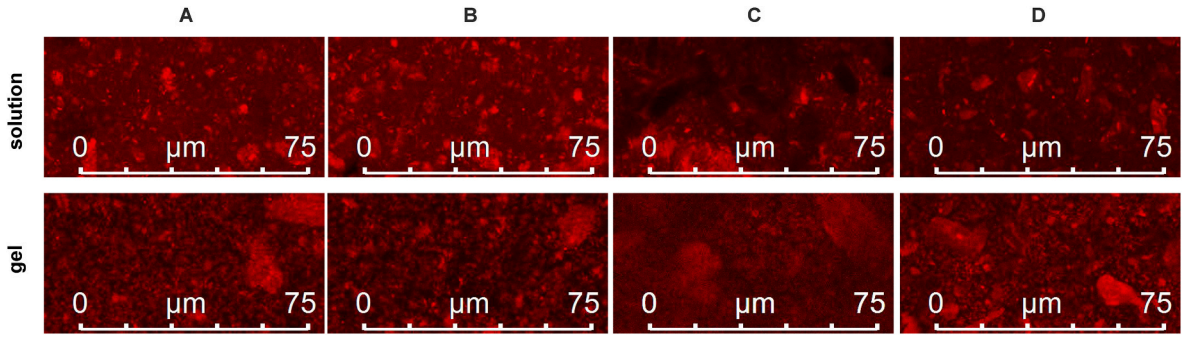

Fig. 9. CLSM microscopy of mealworm protein solutions and gels with and without the addition of 0.3 M ions at a protein concentration of 13.4 % at 63x magnification. Protein was stained with rhodamine B. (A = reference, B=NaCl, C=$MgCl_2$, D = $CaCl_2$).

concentrations of incorporated proteins and denser networks based on more regular structure elements, rheological moduli increase upon addition of (divalent) cations.

The proposed structural differences in aggregation and network structure are reflected in CLSM micrographs (Fig. 9) and rheological behaviour outside the linear viscoelastic regime. characterisation as discussed later. In solution, the addition of divalent cations leads to a decrease in fluorescence intensity as indicated by the pictures and the higher gain required, which might be caused by similar effects as seen in fluorescence spectroscopy and might be related to more pronounced aggregation. This is in agreement with the occurrence of more coarse structures in the corresponding pictures. Upon heat induced gelation, the samples formed a particulate network structure that is finer stranded for the reference and the samples with added NaCl and less homogenous with more/larger flocs for the samples with divalent cations, thus further supporting the findings described above.

3.6. Heat and cation induced changes to rheological behaviour outside the linear viscoelastic regime

It is expected that the observed structural differences in the various gels will also influence their rheological properties at larger deformations. At low intercycle deformations γ_0 the elastic Lissajous curves display a very narrow ellipsoid shape while the viscous Lissajous

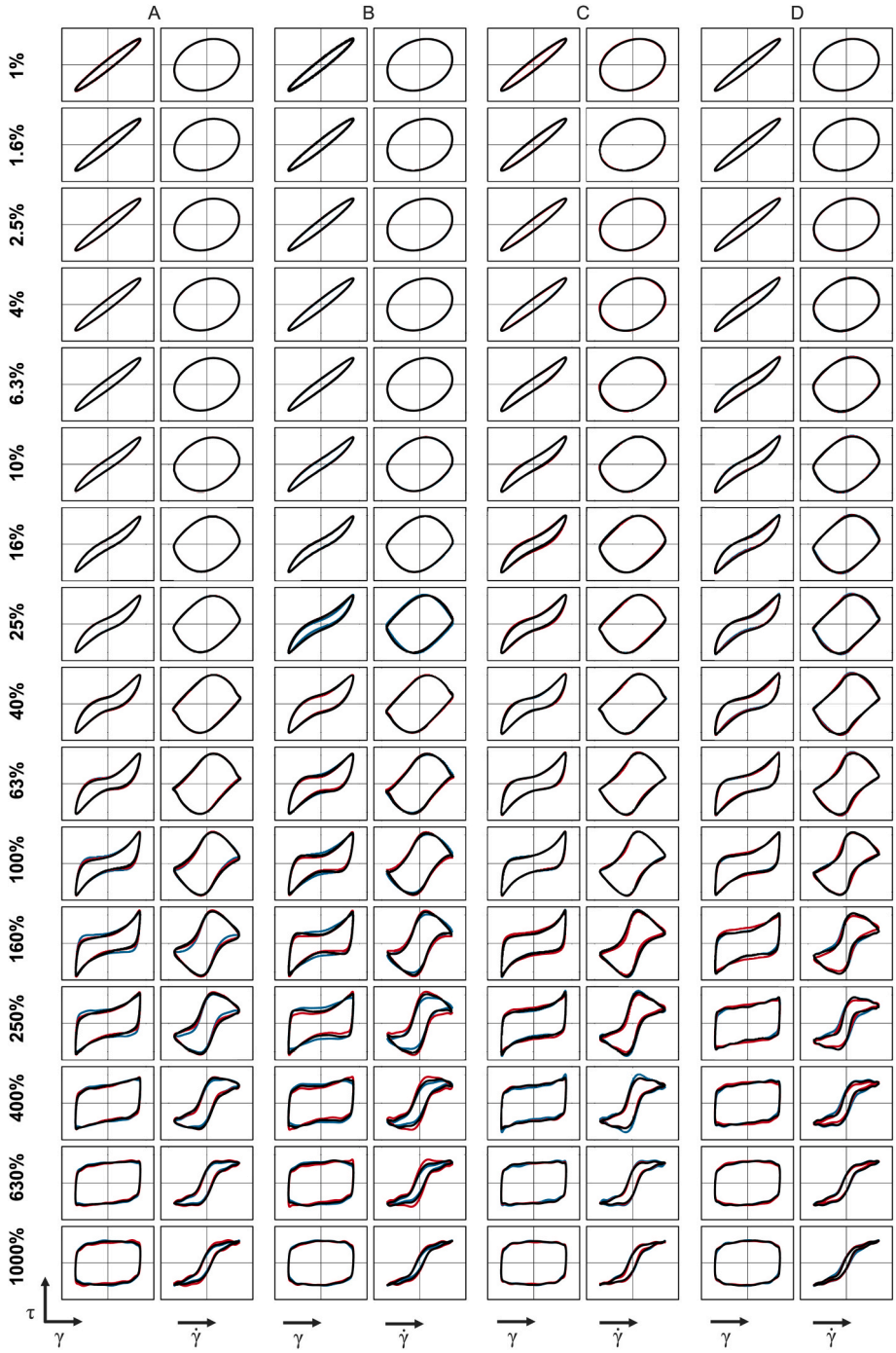

Fig. 10. Standardized elastic and viscous Lissajous curves of mealworm protein gels with and without the addition of 0.3 M ions at a protein concentration of 13.4 % at various intercycle deformations within and outside the linear viscoelastic region. (A = reference, B=NaCl, C=$MgCl_2$, D = $CaCl_2$).

curves have the shape of wide ellipses (Fig. 10). At the same time G', G'', dissipation ratio φ, *S- and T-factors* remain constant (Fig. 11), collectively indicating linear viscoelastic behaviour.

At intercycle strains γ_0 above 2–3 % (reference and sample with NaCl) or 1 % (samples with $MgCl_2$ and $CaCl_2$) storage and loss moduli G' and G'' begin to decrease (Fig. 11). This indicates an overall intercycle strain softening behaviour (Hyun et al., 2002), indicative of a transition toward nonlinear rheological behaviour and is accompanied by the onset of an increase of the dissipation ratio φ as well as by emerging distortion of the Lissajous curves which indicates the beginning contribution of higher harmonics. The increased dissipation ratio φ represents the dissipation of more energy within each oscillation cycle and therefore a shift towards a more viscous or plastic behaviour (Ewoldt et al., 2010), which may be related to irreversible disruption of the protein network structure. At intercycle deformations γ_0 between 1 and 10 %, the disruption of the network structure is only minor, and is reflected in the elastic Lissajous curves as a decrease in the slope of intracycle stress τ at low intracycle strain γ and an increase of slopes in the intracycle stress τ at high intracycle strain γ (Fig. 10). Consequently, the *S-factor* increases, thus indicating intracycle strain stiffening (Ewoldt et al., 2008) (Fig. 11). This may be related to a beginning reduction of size and volume fraction of the overall gel structure (Park et al., 2015). Consequently, smaller gel fractions emerge. These fractions most likely initially (i.e. at intercycle deformations γ_0 just outside the linear viscoelastic regime) still consist of multiple flocs interconnected by interfloc interactions. At the same time, in the viscous Lissajous curves this beginning rupture of the network structure leads to a decrease in the slope of intracycle stress τ at larger intracycle shear rates $\dot{\gamma}$ (see viscous Lissajous curves in Fig. 10), and therefore to intracycle shear thinning as indicated by the decrease in *T-factors* (Ewoldt et al., 2008) (Fig. 11). This intracycle shear thinning can be related to an increase in the flexibility of the remaining gel fragments, which become more capable of aligning in the flow.

At higher intercycle strains γ_0 between 10 % and 100 %, G' and G'' decrease steeply and eventually cross each other (Fig. 11) while the increasing distortion of the Lissajous curves (Fig. 10) indicates an increasing influence of higher harmonics. In this amplitude range the dissipation ratio φ and the *S-factor* begin to increase more steeply and the decrease in *T-factor* and changes to the Lissajous curves (Fig. 10) are also more distinct.

As the deformation increases even further to intercycle strains γ_0 between 100 % and 1000 %, the dissipation ratio φ increases steeply and ultimately converges toward a value just below $\varphi = 1$ (Ewoldt et al., 2010), indicating a transition to a larger contribution of plastic behaviour. This is in agreement with the transition of elastic Lissajous curves toward rectangular, albeit slightly bulbous shapes and the narrowing of the viscous Lissajous curves, which approach a shape between a diagonal line and a vertical increase at zero intracycle strain rate $\dot{\gamma}$ combined with constant stress at larger intracycle strain rates $\dot{\gamma}$. The former would be indicative of purely viscous behaviour, while the latter would represent purely plastic behaviour. Additionally, the *S-factors* divert towards $S = 1$, which is an additional indicator for ideal plastic

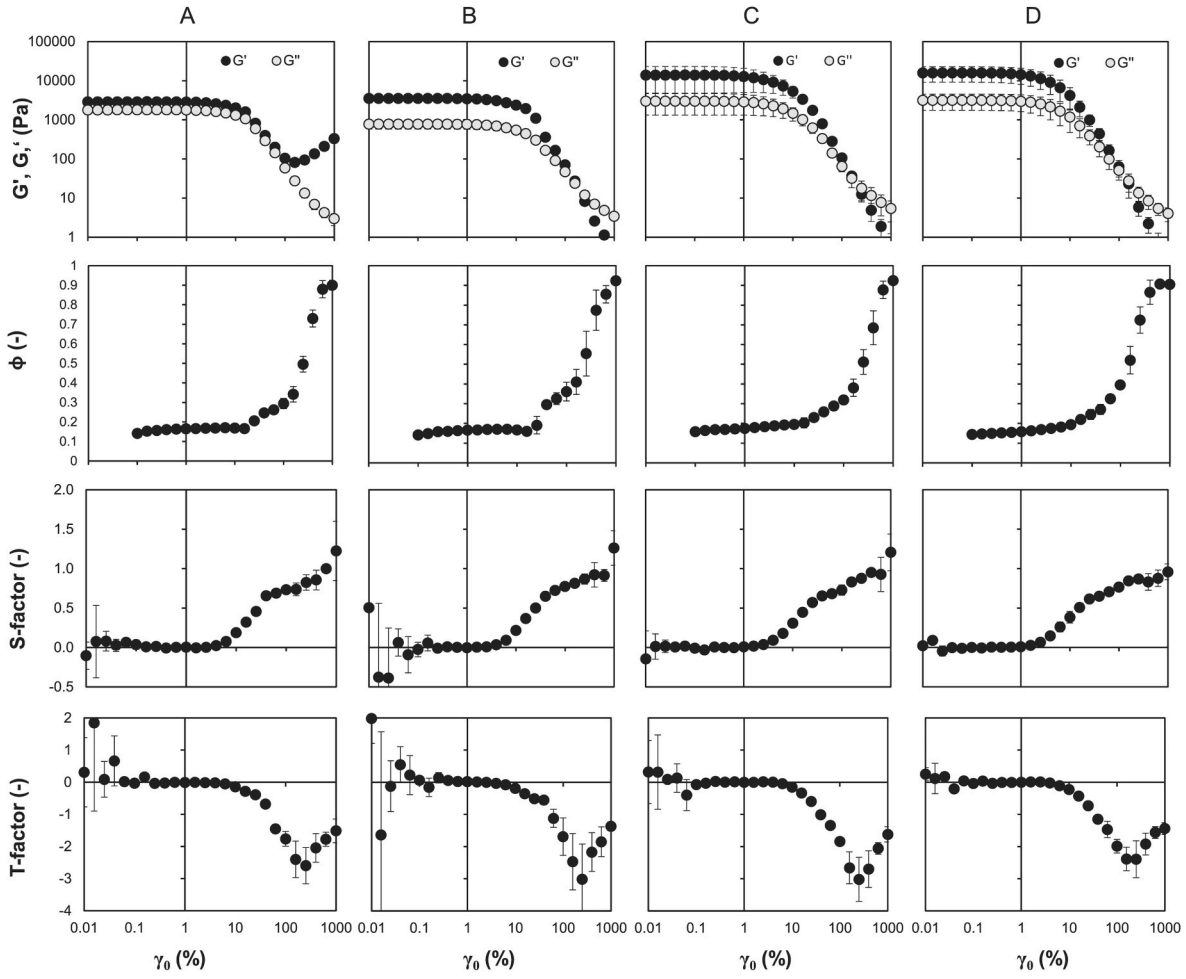

Fig. 11. Various parameters derived from amplitude sweeps of mealworm protein gels with and without the addition of 0.3 M ions at a protein concentration of 13.4 % performed at f = 1Hz plotted over the intercycle deformation γ_0. Top row: storage and loss moduli G′ and G′′, second row: dissipation ratio φ, third row: S-factor and bottom row: T-factor. (A = reference, B=NaCl, C=$MgCl_2$, D = $CaCl_2$).

behaviour, since in this case the G'_M converges towards zero, as is the case for a rectangular Lissajous curve. At the same time, the *T-factor* increases in agreement with the slopes in the viscous Lissajous curves. Consequently, from the combination of dissipation ratio φ, the *S-factor*, the *T-factor*, the development of the shape of elastic and viscous Lissajous curves and the very small area enclosed in the viscous Lissajous curves we propose a mainly visco-plastic behaviour for the gels at very high intercycle strain γ_0 above 400 %. However, for intercycle strains γ_0 in this range artefacts like wall slip cannot be entirely ruled out, since an increase in *T-factor*, when the other parameters converge towards 1, indicating plastic behaviour is to some extent counter indicative, since for plastic behaviour, the *T-factor* should converge towards -∞.

Differences between the observed rheological behaviour of samples with addition of different salts can to some extent be related to the above discussed underlying structures in these samples. This is especially the case at intercycle deformations γ_0 just outside the linear viscoelastic regime (1 % < γ_0 < 10 %). As mentioned above, deviations from linear viscoelastic behaviour occur sooner and are more pronounced in samples with added salt in the order reference < Na^+ < Mg^{2+} < Ca^{2+}. This is in agreement with all previous results such as absorption at 290 nm and G' that imply more pronounced aggregation, protein incorporation and a network density to be influenced by the addition of salts in the same order. Consequently, it appears reasonable to assume an influence of the formed aggregates and their interaction behaviour on the intracycle rheological behaviour of the samples outside the linear viscoelastic regime. More specifically, this behaviour may be related to the observed higher density of original aggregates in samples containing divalent salts as indicated by scattering exponents from SAXS measurements and the larger contribution of intrafloc interactions as reflected by the α-values. In combination, these findings imply an increased stabilisation of the flocs and can lead to a higher susceptibility of interfloc interactions to break upon increasing strain. This may be particularly evident for the samples with $CaCl_2$. The lack of transition from mass fractal to surface fractal upon heating indicates a gel structure, that is dominated by the aggregate building blocks and most susceptible to disruption of interfloc interactions.

At larger deformations (γ_0 > 10 %) differences between samples become smaller and all samples displayed a relatively similar non-linear behaviour under those conditions. This implies only a minor influence of the respective ions and their corresponding impact on protein-, aggregate- and gel structure under conditions where this structure becomes severely mechanically damaged. This may be related to similar interactions contributing to the stabilisation of the overall structure and their stability against mechanical impact.

4. Conclusions

Our study contributes to a better understanding of the influence of mono- and divalent cations on heat induced gelation of proteins from mealworm on various structural length scales. On the molecular level, we were able to show increased intermolecular β-sheet formation, and therefore hydrogen bonding with (divalent) cations. On the floc level, these cations induced more pronounced aggregation as well as the formation of regular structural elements and led to overall denser aggregates with larger fractal dimensions, that subsequently formed denser gels with higher storage moduli and a larger contribution of intrafloc interactions to the rheological behaviour of the gels. These findings may be used to better predict the behaviour of mealworm protein in gel-based food applications and provides an insight into the effect of other food constituents like (divalent) salts on these gels. At the same time, results may be used to customise gel properties of heat-induced mealworm protein gels by targeted addition of selected salts. However, food usually contains further ingredients (e.g. carbohydrates and fats) that may influence the gelation of mealworm protein in different ways. Consequently, further research should focus on the investigation of combinations of between mealworm protein and these ingredients. Additionally, from a mechanistic point of view further research should focus on the contribution of individual protein fractions to the observed effects to further elucidate on the underlying mechanisms.

CRediT authorship contribution statement

Martina Klost: Writing – review & editing, Writing – original draft, Visualization, Investigation, Formal analysis, Conceptualization. **Sarah Gleisenberg:** Investigation. **Stephan Drusch:** Writing – review & editing, Resources. **Baohu Wu:** Investigation. **Olaf Holderer:** Formal analysis. **Henrich Frielinghaus:** Writing – review & editing. **Stephan Förster:** Writing – review & editing, Resources. **Theresia Heiden-Hecht:** Writing – review & editing, Writing – original draft, Investigation, Formal analysis, Conceptualization.

Funding

This research did not receive any specific grant from funding agencies in the public, commercial, or not-for-profit sectors.

Declaration of competing interest

The authors declare that they have no known competing financial interests or personal relationships that could have appeared to influence the work reported in this paper.

Acknowledgements

The authors gratefully acknowledge the assistance and expertise of Karin Engelbert for CLSM measurements, of Lisa Kühnast for protein extraction, of Jia-Jhen Kang for SEC measurements and of Silvia Heim for skillful support during lab-work.

Appendix A. Supplementary data

Supplementary data to this article can be found online at https://doi.org/10.1016/j.foodhyd.2025.111800.

Data availability

Data will be made available on request.

References

Angelini, T. E., Liang, H., Wriggers, W., & Wong, G. C. L. (2005). Direct observation of counterion organization in F-actin polyelectrolyte bundles. *European Physical Journal E, 16*(4), 389–400. https://doi.org/10.1140/epje/i2004-10097-9

Anitas, E. M. (2020). Small-angle scattering from fractals: Differentiating between various types of structures. *Symmetry, 12*(1), 1–31. https://doi.org/10.3390/SYM12010065

Asakereh, I., Lee, K., Francisco, O. A., & Khajehpour, M. (2022). Hofmeister effects of group II cations as seen in the unfolding of ribonuclease A. *ChemPhysChem, 23*(12). https://doi.org/10.1002/cphc.202100884

Beaucage, G. (1996). Small-angle scattering from polymeric mass fractals of arbitrary mass-fractal dimension. *Journal of Applied Crystallography, 29*(2), 134–146. https://doi.org/10.1107/S0021889895011605

Chronakis, I. S. (2001). Gelation of edible blue-green algae protein isolate (Spirulina platensis strain Pacifica): Thermal transitions, rheological properties, and molecular forces involved. *Journal of Agricultural and Food Chemistry, 49*(2), 888–898. https://doi.org/10.1021/jf0005059

Deacon, G. B., & Phillips, R. J. (1980). Relationships bteween the carbon-oxygen stretching frequencies of carboxylato complexes and the type of carboxylate coordination. *Coordination Chemistry Reviews, 33*, 227–250.

Duy, C., & Fitter, J. (2006). How aggregation and conformational scrambling of unfolded states govern fluorescence emission spectra. *Biophysical Journal, 90*(10), 3704–3711. https://doi.org/10.1529/biophysj.105.078980

Ewoldt, R. H., Hosoi, A. E., & McKinley, G. H. (2008). New measures for characterizing nonlinear viscoelasticity in large amplitude oscillatory shear. *Journal of Rheology, 52*(6), 1427–1458. https://doi.org/10.1122/1.2970095

Ewoldt, R. H., Winter, P., Maxey, J., & McKinley, G. H. (2010). Large amplitude oscillatory shear of pseudoplastic and elastoviscoplastic materials. *Rheologica Acta, 49*(2), 191–212. https://doi.org/10.1007/s00397-009-0403-7

Frieden, C. (1983). Polymerization of actin: Mechanism of the Mg2+-induced process at pH 8 and 20°C. *Proceedings of the National Academy of Sciences of the United States of America, 80*(21 I), 6513–6517. https://doi.org/10.1073/pnas.80.21.6513

Gerbino, E., Mobili, P., Tymczyszyn, E., Fausto, R., & Gómez-Zavaglia, A. (2011). FTIR spectroscopy structural analysis of the interaction between Lactobacillus kefir S-layers and metal ions. *Journal of Molecular Structure, 987*(1–3), 186–192. https://doi.org/10.1016/j.molstruc.2010.12.012

Glatter, O., & Kratky, O. (1982). *Small anlge x-ray scattering* (1st ed.). Academic Press https://search.worldcat.org/de/title/Small-angle-x-ray-scattering/oclc/9044069.

Goddette, D. W., Uberbacher, E. C., Bunick, G. J., & Frieden, C. (1986). Formation of actin dimers as studied by small angle neutron scattering. *Journal of Biological Chemistry, 261*(6), 2605–2609. https://doi.org/10.1016/s0021-9258(17)35830-1

Gommes, C. J., Jaksch, S., & Frielinghaus, H. (2021). Small-angle scattering for beginners. *Journal of Applied Crystallography, 54*, 1832–1843. https://doi.org/10.1107/S1600576721010293

Hammouda, B. (2010). Analysis of the beaucage model. *Journal of Applied Crystallography, 43*(6), 1474–1478. https://doi.org/10.1107/S0021889810033856

Hyun, K., Kim, S., Ahn, K., & Lee, S. (2002). Large amplitude oscillatory shear as a way to classify the complex fluids. *Journal of Non-newtonian Fluid Mechanics, 107*(1–3), 51–65. https://doi.org/10.4103/2319-4170.165000

Jackson, M., & Mantsch, H. H. (1995). The use and misuse of FTIR spectroscopy in the determination of protein structure. *Critical Reviews in Biochemistry and Molecular Biology, 30*(2), 95–120. https://doi.org/10.3109/10409239509085140

Janssen, R. H., Vincken, J. P., Van Den Broek, L. A. M., Fogliano, V., & Lakemond, C. M. M. (2017). Nitrogen-to-Protein conversion factors for three edible insects: Tenebrio molitor, Alphitobius diaperinus, and Hermetia illucens. *Journal of Agricultural and Food Chemistry, 65*(11), 2275–2278. https://doi.org/10.1021/acs.jafc.7b00471

Kim, T. K., Lee, M. H., Yong, H. I., Jung, S., Paik, H. D., Jang, H. W., & Choi, Y. S. (2020). Effect of interaction between mealworm protein and myofibrillar protein on the rheological properties and thermal stability of the prepared emulsion systems. *Foods, 9*(10). https://doi.org/10.3390/foods9101443

Kim, H. W., Setyabrata, D., Lee, Y. J., Jones, O. G., & Kim, Y. H. B. (2016). Pre-treated mealworm larvae and silkworm pupae as a novel protein ingredient in emulsion sausages. *Innovative Food Science and Emerging Technologies, 38*, 116–123. https://doi.org/10.1016/j.ifset.2016.09.023

Kim, J. H. J., Varankovich, N. V., & Nickerson, M. T. (2016). The effect of pH on the gelling behaviour of canola and soy protein isolates. *Food Research International, 81*, 31–38. https://doi.org/10.1016/j.foodres.2015.12.029

Klost, M., Ramirez-Huerta, M. I., & Drusch, S. (2022). Heat-induced gelation of protein from mealworm (Tenebrio molitor): Influence of pH and zinc concentration. *Food Hydrocolloids for Health, 2*(September), Article 100105. https://doi.org/10.1016/j.fhfh.2022.100105

Lee, H. J., Kim, J. H., Ji, D. S., & Lee, C. H. (2019). Effects of heating time and temperature on functional properties of proteins of yellow mealworm larvae (Tenebrio molitor L.). *Food Science of Animal Resources, 39*(2), 296–308. https://doi.org/10.5851/kosfa.2019.e24

Li Tay, S., Yao Tan, H., & Perera, C. (2006). The coagulating effects of cations and anions on soy protein. *International Journal of Food Properties, 9*(2), 317–323. https://doi.org/10.1080/10942910600596340

Mezzenga, R., & Fischer, P. (2013). The self-assembly, aggregation and phase transitions of food protein systems in one, two and three dimensions. *Reports on Progress in Physics, 76*(4). https://doi.org/10.1088/0034-4885/76/4/046601

Norman, A. I., Ivkov, R., Forbes, J. G., & Greer, S. C. (2005). The polymerization of actin: Structural changes from small-angle neutron scattering. *Journal of Chemical Physics, 123*(15). https://doi.org/10.1063/1.2039088

Oh, E., & Kim, Y. (2024). Influence of mealworms (Tenebrio molitor larvae) and their protein derivatives on the structural and rheological properties of tofu. *Food Hydrocolloids, 147*(September 2023). https://doi.org/10.1016/j.foodhyd.2023.109399

Park, J. D., Ahn, K. H., & Lee, S. J. (2015). Structural change and dynamics of colloidal gels under oscillatory shear flow. *Soft Matter, 11*(48), 9262–9272. https://doi.org/10.1039/c5sm01651g

Pinel, G., Berthelot, U., Queiroz, L. S., Santiago, L. D. A., Silva, N. F. N., Petersen, H. O., Sloth, J. J., Altay, I., Marie, R., Feyissa, A. H., Casanova, F., & Doyen, A. (2024). Influence of the processing on composition, protein structure and techno-functional properties of mealworm protein concentrates produced by isoelectric precipitation and ultrafiltration/diafiltration. *Food Chemistry, 449*(November 2023), Article 139177. https://doi.org/10.1016/j.foodchem.2024.139177

Potter, J. D., & Gergely, J. (1975). The calcium and magnesium binding sites on troponin and their role in the regulation of myofibrillar adenosine triphosphatase. *Journal of Biological Chemistry, 250*(12), 4628–4633. https://doi.org/10.1016/s0021-9258(19)70187-2

Töpperwien, M., Priebe, M., & Salditt, T. (2016). Actin bundles cross-linked with α -actinin studied by nanobeam X-ray diffraction. *European Biophysics Journal, 45*(5), 383–392. https://doi.org/10.1007/s00249-015-1107-9

Vladislav Victorovich, K., Tatyana Aleksandrovna, K., Victor Vitoldovich, P., Aleksander Nicolaevich, S., Larisa Valentinovna, K., & Anastasia Aleksandrovna, A. (2021). Spectra of tryptophan fluorescence are the result of co-existence of certain most abundant stabilized excited state and certain most abundant destabilized excited state. *Spectrochimica Acta - Part A: Molecular and Biomolecular Spectroscopy, 257*, Article 119784. https://doi.org/10.1016/j.saa.2021.119784

Wu, H., & Morbidelli, M. (2001). Model relating structure of colloidal gels to their elastic properties. *Langmuir, 17*(4), 1030–1036. https://doi.org/10.1021/la001121f

Zhao, X., Kim, I., Kim, H., & Kim, Y. (2024). Protein interactions and rheological properties of heat-induced gels containing soy and water-soluble mealworm (Tenebrio molitor larvae) protein mixtures. *Food Bioscience, 58*(November 2023), Article 103718. https://doi.org/10.1016/j.fbio.2024.103718

Zhao, X., Vázquez-Gutiérrez, J. L., Johansson, D. P., Landberg, R., & Langton, M. (2016). Yellow mealworm protein for food purposes - Extraction and functional properties. *PLoS One, 11*(2), 1–17. https://doi.org/10.1371/journal.pone.0147791

Zimmerle, C. T., Patane, K., & Frieden, C. (1987). Divalent cation binding to the High- and low-affinity sites on G-Actin. *Biochemistry, 26*(20), 6545–6552. https://doi.org/10.1021/bi00394a039